

# Real-Time Optical Process Monitoring for Structure and Property Control of Aerosol Jet Printed Functional Materials

Rebecca R. Tafoya, Adam W. Cook, Bryan Kaehr, Julia R. Downing, Mark C. Hersam, and Ethan B. Secor\*

Aerosol jet printing is a popular digital additive manufacturing method for flexible and hybrid electronics, but it lacks sophisticated real-time process control schemes that would enable more widespread adoption in manufacturing environments. Here, an optical measurement system is introduced to track the aerosol density upstream of the printhead. The measured optical extinction, combined with the aerosol flow rate, is directly related to deposition rate and accurately predicts functional materials properties such as the electrical resistance of printed graphene films. This real-time system offers a compelling solution for process drift and batch-to-batch variability, rendering it a valuable tool for both real-time control of aerosol jet printing and fundamental studies of the underlying process science.

The rapid development of digital printing technologies promises to transform manufacturing, offering precise location control and customizable patterning with high resolution.<sup>[1,2]</sup> By applying digital fabrication methods to functional materials, these technologies offer rapid prototyping that can leverage advanced algorithms and controls. However, serial production leads to significant challenges in quality assurance, particularly when the underlying fabrication technologies are vulnerable to stochastic processes that lead to inconsistency. Across digital printing methods a critical need exists for improved in-line process monitoring and control.<sup>[3,4]</sup>

Among printing technologies, aerosol jet printing (AJP) is well-suited for flexible and hybrid electronics fabrication.<sup>[5,6]</sup> AJP uses a focused aerosol stream of a liquid ink to deposit high resolution (10–50  $\mu\text{m}$ ), thin film (typically <10  $\mu\text{m}$ ) patterns of functional materials such as conductive nanoparticles

and dielectric polymers.<sup>[7]</sup> Due to its programmable, non-contact, and versatile nature, AJP has been utilized for a wide range of electronic device applications, including logic circuits,<sup>[8,9]</sup> sensing,<sup>[10,11]</sup> energy conversion,<sup>[12,13]</sup> wireless communication,<sup>[14,15]</sup> and energy storage.<sup>[16]</sup> However, widespread adoption of AJP in industrial manufacturing is uncommon due to its poor process consistency.<sup>[17,18]</sup>

Recent efforts have introduced strategies to mitigate process drift or provide process monitoring capabilities during AJP. For example, in our previous work, we demonstrated that substantial process drift arises due to variations in the


cartridge loading alone, independent of ink composition drift, motivating the introduction of a continuous flow cartridge to address both sources in a passive manner.<sup>[19]</sup> To evaluate the ink deposition rate in near real-time, Hines et al. introduced a strategy for manually calibrating the deposition rate using well-defined microfabricated inkwells.<sup>[17]</sup> Moreover, Salary et al. demonstrated online process monitoring based on optical characterization of lines following deposition.<sup>[20]</sup> While these studies offer strategies for mitigating inconsistency, none have provided robust real-time characterization for process control in an adaptable and generalizable framework. Motivated by a fundamental understanding of AJP, we demonstrate here a printhead and mounted measurement system that allows real-time optical characterization of the aerosol stream. This optical measurement scheme is predictive of functional properties with far greater accuracy than traditional process parameters alone, such as atomizer voltage and gas flow rates. Overall, this approach offers clear benefits for process control in production environments, more thorough insight to investigate the fundamental science of AJP, and real-time characterization of a physically relevant parameter (i.e., the aerosol density) as a viable route to closed-loop control.

In AJP, a liquid ink is atomized to produce micron-scale droplets, which are entrained in a gas flow and carried to the printhead. There, an annular sheath gas collimates the aerosol stream and accelerates it through a nozzle to impact upon a substrate. By moving the substrate relative to the printhead with a numerical control motion system, patterns can be defined in software and printed with feature sizes as fine as  $\approx 10 \mu\text{m}$ . During this process, changes in ink atomization lead to downstream variation in the deposition rate, which can have a secondary effect on print resolution.<sup>[21]</sup> These issues lead to

R. R. Tafoya, A. W. Cook, Dr. B. Kaehr, Prof. E. B. Secor  
Advanced Materials Laboratory  
Sandia National Laboratories  
Albuquerque, NM 87185, USA  
E-mail: esecor@iastate.edu

J. R. Downing, Prof. M. C. Hersam  
Department of Materials Science and Engineering  
Northwestern University  
Evanston, IL 60208, USA

Prof. E. B. Secor  
Department of Mechanical Engineering  
Iowa State University  
Ames, IA 50011, USA

 The ORCID identification number(s) for the author(s) of this article can be found under <https://doi.org/10.1002/admt.202000781>.

DOI: 10.1002/admt.202000781

severe inconsistency, including both sample-to-sample (i.e., process drift) and batch-to-batch variability. To describe variability, we will consider the dry deposition rate (i.e., volume of solids deposited per unit time, measured following printing and curing). In principle, the dry deposition rate can be described as:

$$r_{\text{dep}} = v_a f_a \chi_s (1 - \phi) \eta_{\text{imp}} \quad (1)$$

in which  $r_{\text{dep}}$  is the deposition rate,  $v_a$  is the aerosol density (i.e., volume fraction of liquid in liquid-gas aerosol),  $f_a$  is the aerosol flow rate,  $\chi_s$  is the solids volume fraction of the ink,  $\phi$  is the film porosity, and  $\eta_{\text{imp}}$  is the impaction efficiency. Although the impaction efficiency can change at extreme flow rate conditions, it remains relatively constant under normal operation.<sup>[22]</sup> Similarly, film porosity is likely to be fairly consistent under normal conditions, with variation expected at extremes of the focusing ratio (i.e., the ratio of sheath gas to aerosol carrier gas flow rates). Because the ink solids fraction is also fixed in each experiment, this parameter will similarly not be considered a primary contributor to process variability. Under these conditions, two principal parameters remain: the aerosol flow rate and the aerosol density. While the aerosol flow rate is digitally programmed and regulated by a mass flow controller, the aerosol density is a result of complex interactions related to ink atomization and aerosol transport. Because aerosol density was implicated in earlier studies to understand process drift,<sup>[19]</sup> this parameter is identified here to be poorly controlled, providing a compelling target for in-line monitoring.

To monitor aerosol density in real time during printing, we designed a printhead with an integrated optical port to enable optical extinction measurements (Figure 1a). Previous work to visualize the aerosol stream exiting the print nozzle revealed substantial optical scattering from the micron-scale droplets,<sup>[23]</sup> forecasting the opportunity for quantitative measurements. To test whether this system is sensitive enough to detect variations in the optical density of the aerosol stream, a proof-of-concept experiment was performed. A conductive graphene ink containing 1% w/v graphene/ethyl cellulose solids in 9:1 ethanol:terpineol v/v was used, with a solvent bubbler

upstream of the cartridge to mitigate composition drift over long durations. As shown in Figure 1b, a series of films was printed with varying atomizer voltage. The resulting optical extinction measurements indicate troughs in the signal at the beginning and end of each printed sample, as the aerosol flow and atomizer power were zeroed after each sample to return to baseline. In addition, features corresponding to fine process adjustments can be observed, such as the cartridge equilibration while printing the first sample, which results in a rougher film (Figure S1, Supporting Information). Moreover, analysis of the printed film thickness indicates a correlation with the real-time optical measurement. This observation supports the viability of this measurement configuration, not only to detect discrete or qualitative changes in the aerosol stream (i.e., on/off operation), but to measure continuous, quantitative changes that can be predictive of functional properties downstream.

A thorough experiment was designed to evaluate the real-time optical measurement system for process monitoring. As shown in Figure 2a, the aerosol density (corresponding to atomization efficacy of the ink) is influenced by a wide range of process parameters, including the cartridge fill level, atomizer voltage, aerosol flow rate, ink composition, cartridge temperature, and pressure. The primary process metric dictated by aerosol density is the deposition rate, although it is expected to also have indirect effects on the resolution and microstructure.<sup>[21]</sup> Therefore, this study focuses on the region defined by the grey dashed line in Figure 2a. A series of experiments was developed, each for a defined initial cartridge loading from 0.5–1.0 mL, as shown in Figure 2b. In each case, 4 atomizer voltages and 6 aerosol flow rates were used in a combinatorial manner, resulting in 24 printed samples with a randomized order (the sheath flow rate was adjusted to maintain a focusing ratio of 3 for all experiments). In addition, during printing the cartridge was cleaned and refilled after each set of 8 samples to mitigate composition drift of the ink, and an initialization print for 5 min was performed to ensure equilibration of the cartridge prior to printing any samples. For each sample, the atomizer and aerosol flow were activated  $\approx 50$  sec prior to the start of printing, and deactivated immediately following printing,

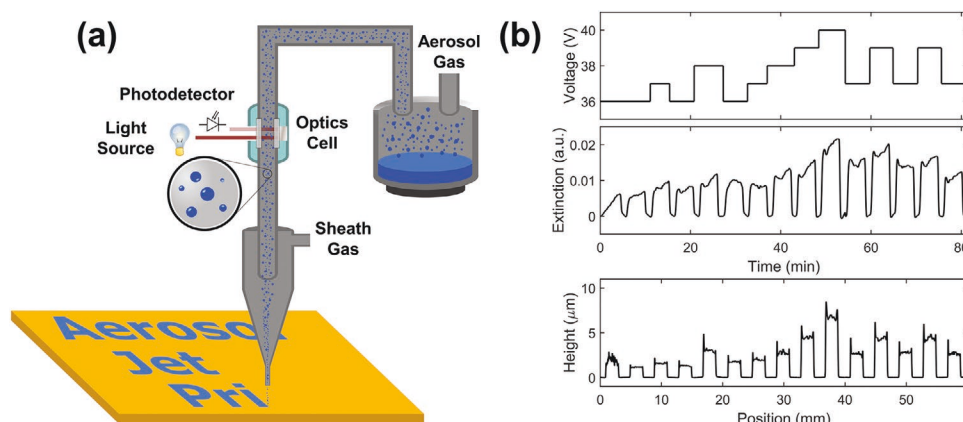


**Figure 1.** Demonstration of optical measurement system for real-time process monitoring. a) Schematic illustration of the optical measurement system, which uses a custom printhead with an optics cell, light source, and photodetector to characterize the aerosol upstream of the printhead. b) Proof-of-concept demonstration of the optical system, showing correlated data for the atomizer voltage, the real-time measurement of optical extinction, and the final film thickness following curing.

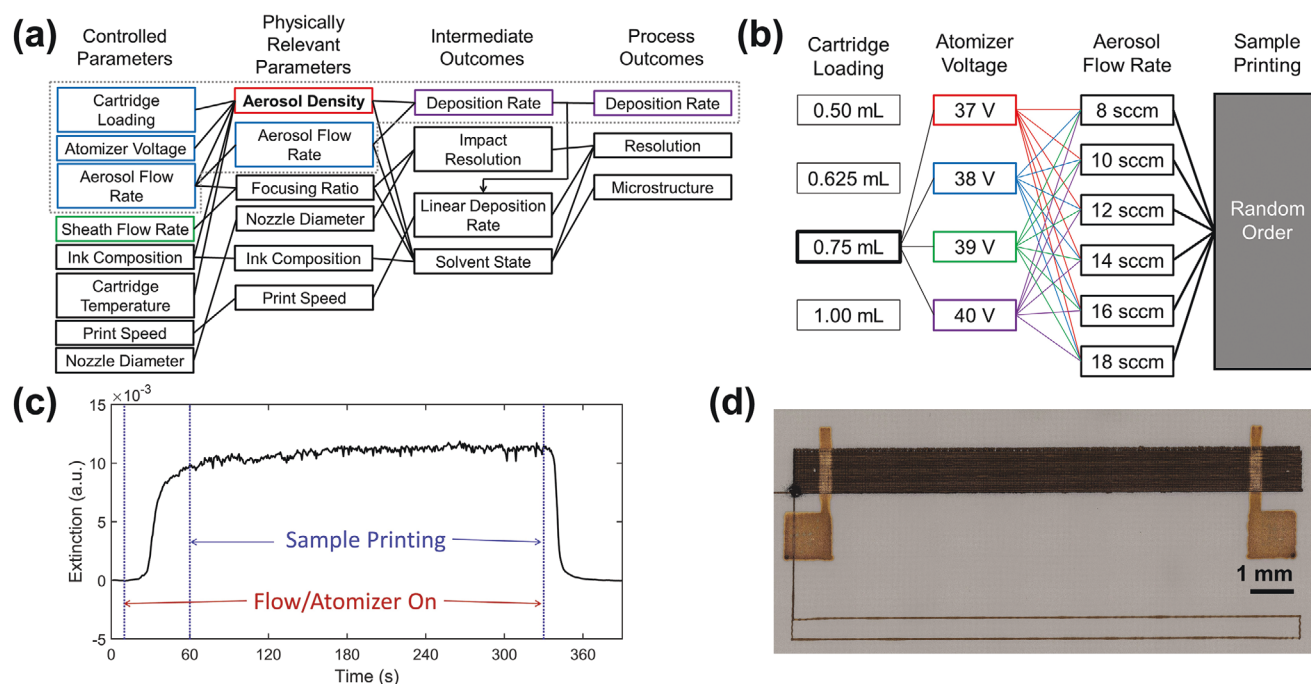


**Figure 2.** Experimental design framework for testing the process monitoring system. a) Description of relevant process parameters during printing, indicating that the controlled parameters do not always directly correlate with those that are physically relevant. b) Experimental design to test the system, with a primary focus on the deposition rate. Cartridge loading, atomizer voltage, and aerosol flow rate were investigated, and for each cartridge loading the order of experiments was randomized to control for drift in ink composition. c) Representative optical data for a single sample, showing the experimental sequence. d) Microscopy image showing the layout of a single test sample.

to provide a baseline for the optical measurement (Figure 2c). We note that some drift in the baseline was evident, likely due to changes in the ambient temperature, so baseline subtraction was performed during analysis (Figure S1b, Supporting Information).

Using the graphene ink described above, the optical measurement signal can be correlated to a functional property of printed patterns, namely electrical conductance, which is directly linked to the amount of material deposited; in contrast, a metric such as thickness could vary depending on film microstructure. A standard resistor geometry was used, with a  $1 \times 12$  mm bar of graphene printed first followed by printed silver contact pads (Figure 2d). Following printing, all samples were cured on a hotplate at  $325^\circ\text{C}$  for 1 h prior to characterization. Four-point probe resistance measurements were collected, along with film cross-sectional area and microscopy images. In total, 96 samples were printed and characterized (Figure S2,S3, Supporting Information, Discussion 1). Of the eight samples printed upon each refresh of the ink cartridge, the first five (corresponding to  $\approx 30$  min of printing) were used for further analysis to avoid confounding effects of drift in the ink composition (Figure S3d, Supporting Information, Discussion 1).

While users of AJP are typically constrained to calibration based on the directly controlled parameters (i.e., atomizer voltage and aerosol flow rate), these parameters do not account for variability in ink atomization and are thus poor predictors of functional properties, such as conductance (Figure 3a). On the other hand, regardless of the cartridge fill level, the conductance features a clear, approximately linear correlation with the real-time process metric (Figure 3b), defined here

as the product of optical extinction and aerosol flow rate following Equation (1). The two-way correlation matrix for this data set indicates an outstanding fit for the process metric, with a coefficient of 0.97 (Figure 3c), thus establishing the predictive accuracy of this real-time process monitoring capability for functional properties. Moreover, while this data set maintains a focusing ratio of 3 for consistency, an independent experiment confirms the applicability of this linear fit even when the focusing ratio is varied (Figure S4, Supporting Information). This process metric provides insight into the printing process beyond the downstream property of conductance alone. When the film conductivity, the bulk material property which normalizes conductance to sample geometry, is plotted against the product of aerosol flow rate and optical extinction, three distinct regimes emerge (Figure S5, Supporting Information). At very low values of the real-time metric, films are not conductive. In an intermediate transition zone, the conductivity exhibits wide variability as it approaches a plateau. For high values of the metric (corresponding to high deposition rates) the conductivity reaches a stable plateau near  $35000\text{ S m}^{-1}$ . Under these conditions, deposition of a wet film allows flakes to form a dense microstructure, as compared to dry deposition in a solvent-poor state (Figure S6, Supporting Information). This insight based on the process metric therefore allows improved print optimization based on film conductivity, which is related to microstructure, rather than conductance alone, which could be relevant for applications in which porosity and surface area are important.<sup>[24,25]</sup>

The quality of the process metric as a predictor for functional properties provides an opportunity for process control.

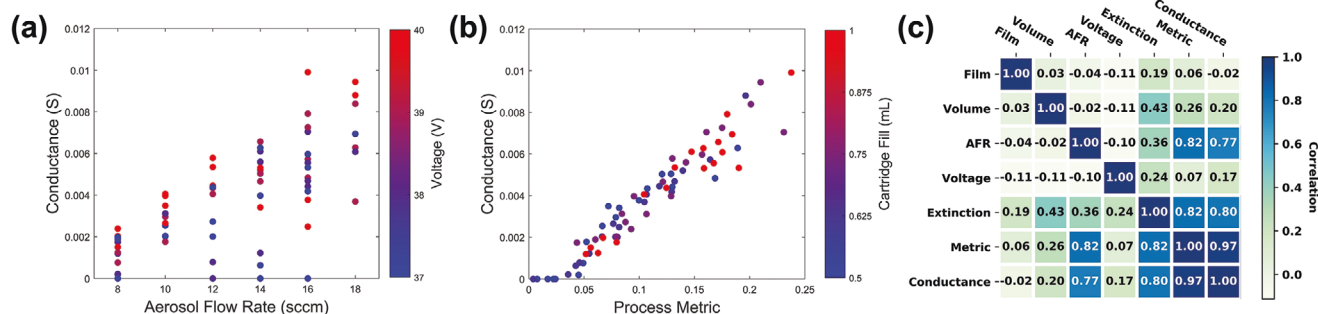


**Figure 3.** Data analysis for graphene resistors. a) Sample conductance plotted against aerosol flow rate for the subset of 60 samples, showing poor predictive accuracy based on standard process parameters. The color scale corresponds to the atomizer voltage in this plot. b) Sample conductance plotted against the process metric, the product of aerosol flow rate and average optical extinction. The color scale indicates the cartridge fill volume, showing that this metric is robust even with varying fill volume. c) Two-way correlation matrix for the data subset including the relevant process parameters of film number, cartridge fill volume, aerosol flow rate (AFR), atomizer voltage, optical extinction, process metric, and conductance. The values and color scale correspond to the linear correlation,  $r^2$ , revealing an outstanding fit of 0.97 for the process metric.

To illustrate this potential, a pseudo-closed-loop system with manual control was utilized to print resistors with targeted functional properties. As shown above, the process metric is an excellent predictor of electrical resistance given a fixed pattern. To target resistances over a wider range, a simple model was developed to relate the process metric and pattern parameters with sample resistance (Supporting Information, Discussion 2). In this case, each resistor is printed with two layers, and the optical measurement from the first layer is used to adjust the print speed for the second layer, thus modulating the amount of material deposited. This process flow is shown schematically in Figure 4a. Resistance values of 200, 400, 600, and 1000  $\Omega$  were targeted, with a linear fit assumed between the process metric and the deposition rate. Following printing and post-processing, the resistance values matched closely with the initial targets, as shown in Figure 4b. Increased deviation between the actual and predicted resistance at high values (1000  $\Omega$ ) suggests that the true linearity of the fit may be an inadequate assumption far from the calibration data. More importantly, for each set of resistors the actual resistance was reasonably consistent despite variation in the optical extinction measurement, illustrating the necessity to account for that variation by adjusting the print speed. This analysis illustrates the value of a real-time metric for more sophisticated process control. Notably, print speed was selected as the control parameter because it is not expected to affect printing mechanisms upstream of the print nozzle. The aerosol flow rate, which may seem a logical choice given its inclusion in Equation (1), has a nonlinear effect. This is demonstrated by the positive correlation between aerosol flow rate and optical extinction, which aligns with prior fundamental work describing aerosol settling within the mist tube.<sup>[7]</sup> Because changes in aerosol flow rate would affect both parameters comprising the process metric in a difficult to predict manner, the print speed is a clear choice for modulating the linear deposition rate, or deposition rate normalized to print speed,<sup>[21]</sup> with minimal effect on the upstream physical processes.

Because the optical response depends on light scattering from aerosol droplets, these compelling results for graphene should be generalizable to other inks. This hypothesis was validated with poly(methyl methacrylate) (PMMA) and

magnetite nanoparticle inks. For these non-conductive inks, film thickness was used as the indicator of the deposition rate. Similar experiments were conducted varying both the atomizer voltage and the aerosol flow rate, maintaining a focusing

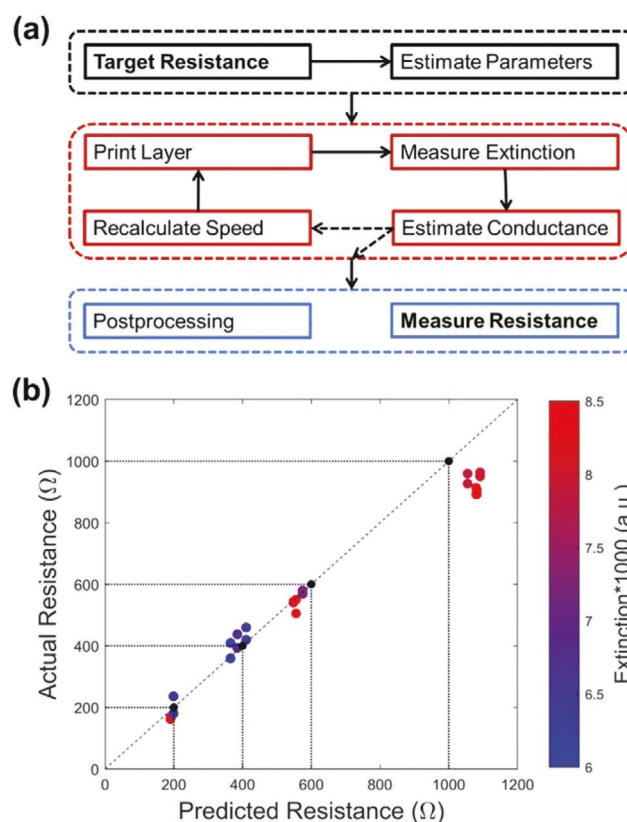


**Figure 4.** Process control framework for printing with targeted electrical properties. a) Experiment design to test printing of multilayer resistors, in which the print speed can be modified after each layer to achieve a targeted resistance value. In this case, only two layers were used. b) Results of the experiment for graphene resistors, showing the actual resistance plotted against predicted resistance. The dashed lines indicate the target resistance values, and the color scale illustrates the aerosol density, showing that although it changed during printing a suitable fit to the target was maintained.



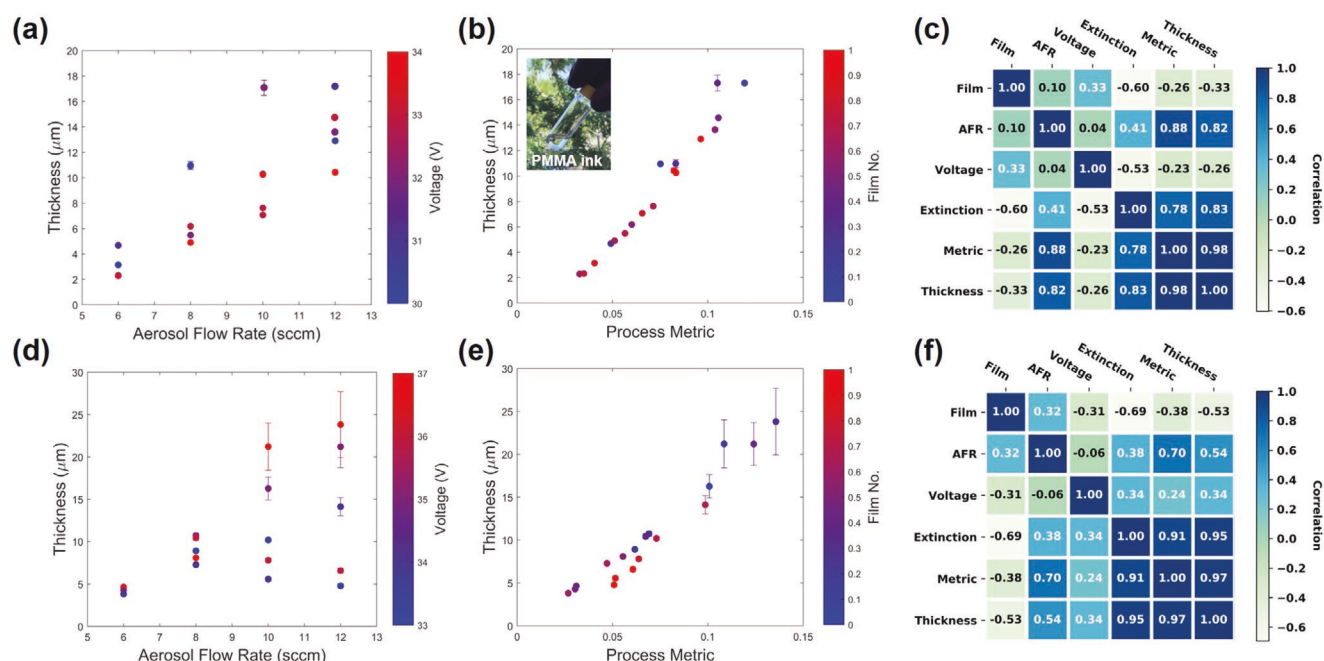


**Figure 5.** Generalization of real-time process monitoring. Analysis of data for a PMMA ink, including a) variation in thickness with standard parameters of flow rate and voltage, b) variation with the process metric, the product of aerosol flow rate, and optical extinction, and c) the two-way correlation matrix summarizing the relationships between process variables. The inset image in (b) is a photograph of the PMMA ink vial, illustrating the optical transparency of the ink. d–f) Corresponding data for a magnetite nanoparticle ink.

ratio of 3. PMMA was selected for its optical transparency, to demonstrate that this method works based on light scattering, and is applicable in the absence of optical absorption. As shown in **Figure 5**, and suggested by Equation (1), the product of the optical extinction and aerosol flow rate shows a highly linear relationship with the thickness measured following printing. Notably, during these experiments the ink was not replaced for over 2 h of printing. While significant drift is observed in the deposition rate over time (Figure S7, Supporting Information), because the ink composition varies minimally, the relation between thickness and the process metric is maintained with high accuracy, with a correlation coefficient of 0.98 and 0.97 for PMMA and magnetite inks, respectively.

The compelling results demonstrated here reflect a confluence of insights. First, this work builds on a fundamental understanding of the AJP process, including sources of process drift. It leverages this scientific basis to identify the primary, physically-relevant AJP process parameter that is not directly controlled in the process (i.e., the aerosol density). A custom printhead and measurement system were then designed exclusively to track this parameter in real time. This tool offers clear advantages for reducing within- and between-batch variability in production environments, overcoming a clear practical challenge for more widespread adoption of AJP. As demonstrated here, this approach can use the average optical extinction measured during printing. However, this optical signal can also be useful on shorter timescales, with or without a baseline. We demonstrate that the short-term variability of the optical signal, which can be measured without stopping printing to collect a baseline, is also a useful, real-time process metric (Figure S8,

Supporting Information). In addition, elimination of drift in the measurement signal, related to the light source, would support more sophisticated control based on this technology. This tool results in a feature-rich data record for print validation, which can be used to support a digital twin and machine learning models for, among other purposes, quality assurance. Moreover, it provides insight into physical mechanisms not possible with post-printing characterization alone, offering a path to improved process understanding by offering a direct measure of the aerosol state within the printhead. As a non-invasive, real-time process monitoring capability with straightforward automation, this scheme provides a viable route to closed-loop control and more sophisticated digital printing architectures. Overall, this work provides a valuable and generalizable tool to support process monitoring in production environments, basic research for more thorough scientific understanding, and a route to closed-loop control for AJP.

## Experimental Section

**Materials:** All solvents were obtained from Millipore-Sigma. A powder containing graphene with ethyl cellulose was prepared following previously established protocols.<sup>[26,27]</sup> High shear mixing of graphite in an ethanolic solution of ethyl cellulose (4 cP grade, Sigma-Aldrich) exfoliated graphene flakes, which were isolated by centrifugation and flocculation in salt water (0.04 g mL<sup>-1</sup>). The resulting powder, containing 45 wt.% graphene, was dispersed in a 9:1 v/v mixture of ethanol and terpineol at a total solids loading of 10 mg mL<sup>-1</sup> by bath sonication. For the PMMA ink, poly(methyl methacrylate) ( $M_w \approx 15000$ ) was dissolved at a concentration of 10 mg mL<sup>-1</sup> in a 9:1 mixture of xylenes and terpineol by mixing at room temperature. The magnetite ink was obtained from

UT Dots, Inc. A thick paste containing magnetite nanoparticles (UTD-MI-SD) was diluted 1:4 w/w with xylenes. This stock solution was mixed with xylenes and terpineol in a 5:31:4 v/v ratio (stock:xylenes:terpineol) to prepare the ink.

**Aerosol Jet Printing:** Printing experiments were performed using a custom-built aerosol jet printer. The cartridge temperature, substrate temperature, print nozzle diameter, and print speed were maintained at 20 °C, 60 °C, 200 µm, and 2.5 mm s<sup>-1</sup>, respectively. For graphene printing, prior to each set of 8 samples the cartridge was cleaned, refilled with ink, and equilibrated during 5 min of printing. Unless specified otherwise, the sheath gas flow rate was varied to maintain a sheath to aerosol carrier gas flow rate ratio of 3. Before and after printing each sample, the atomizer and aerosol flow were deactivated to collect the baseline optical signal. Following printing, graphene samples were heated in air on a hotplate to 325 °C for 1 h to cure the ink; PMMA and magnetite samples were heated to 150 °C for 1 h.

**Characterization:** Optical microscopy images were collected using a Keyence VHX-7000 digital microscope with 100x magnification. Sample cross section area was measured using a Bruker Dektak XT stylus profilometer with 3.0 mg force and a scan speed of 0.5 mm s<sup>-1</sup>. In each case, three measurements were collected per sample. Resistance measurements were collected using a Keithley 2450 source meter with a 4-probe measurement configuration.

**Optical Measurements:** A Thorlabs SLS201L fiber-coupled light source was used for the optical measurements. Optical transmission measurements were performed in a reflection configuration (as shown in Figure 1a), with the reflected light directed to a Thorlabs S155C photodiode. Data was monitored in real time and logged using a custom program written in Python. An optics cell was 3D printed using stereolithography and was integrated directly on the printhead (Figure S9, Supporting Information). Quartz optical windows provided an optically clear path for the incident and reflected light, and these windows were set back from the primary aerosol path to prevent accumulation of ink on the windows.

## Supporting Information

Supporting Information is available from the Wiley Online Library or from the author.

## Acknowledgements

This work was generously supported by the Harry S. Truman Fellowship, through the Laboratory Directed Research and Development program at Sandia National Laboratories, and was performed in part at the Center for Integrated Nanotechnologies, an Office of Science User Facility operated for the U.S. Department of Energy (DOE) Office of Science. Graphene ink preparation was supported by the National Science Foundation (NSF) Scalable Nanomanufacturing Program (NSF Award Number CMMI-1727846). Sandia National Laboratories is a multi-program laboratory managed and operated by National Technology and Engineering Solutions of Sandia, LLC, a wholly owned subsidiary of Honeywell International, Inc., for the U.S. Department of Energy's National Nuclear Security Administration under contract DE-NA-0003525. This paper describes objective technical results and analysis. Any subjective views or opinions that might be expressed in the paper do not necessarily represent the views of the U.S. Department of Energy or the United States Government.

## Conflict of Interest

The authors declare no conflict of interest.

## Keywords

additive manufacturing, aerosol jet printing, printed electronics, process control

Received: August 7, 2020

Revised: September 23, 2020

Published online: November 9, 2020

- [1] S. H. Huang, P. Liu, A. Mokasdar, L. Hou, *Int. J. Adv. Manuf. Technol.* **2013**, 67, 1191.
- [2] T. D. Ngo, A. Kashani, G. Imbalzano, K. T. Q. Nguyen, D. Hui, *Composites, Part B* **2018**, 143, 172.
- [3] S. K. Everton, M. Hirsch, P. Stravroulakis, R. K. Leach, A. T. Clare, *Mater. Des.* **2016**, 95, 431.
- [4] M. Grasso, B. M. Colosimo, *Meas. Sci. Technol.* **2017**, 28, 044005.
- [5] Y. Khan, A. Thielens, S. Muin, J. Ting, C. Baumbauer, A. C. Arias, *Adv. Mater.* **2020**, 32, 1905279.
- [6] N. J. Wilkinson, M. A. A. Smith, R. W. Kay, R. A. Harris, *Int. J. Adv. Manuf. Technol.* **2019**, 105, 4599.
- [7] E. B. Secor, *Flexible Printed Electron.* **2018**, 3, 035002.
- [8] C. Cao, J. B. Andrews, A. D. Franklin, *Adv. Electron. Mater.* **2017**, 3, 1700057.
- [9] M. Ha, J. W. Seo, P. L. Prabhumirashi, W. Zhang, M. L. Geier, M. J. Renn, C. H. Kim, M. C. Hersam, C. D. Frisbie, *Nano Lett.* **2013**, 13, 954.
- [10] K. Parate, S. V. Rangnekar, D. Jing, D. L. Mendivelso-Perez, S. Ding, E. B. Secor, E. A. Smith, J. M. Hostetter, M. C. Hersam, J. C. Claussen, *ACS Appl. Mater. Interfaces* **2020**, 12, 8592.
- [11] S. Vella, C. S. Smithson, K. Halfyard, E. Shen, M. Chrétien, *Flexible Printed Electron.* **2019**, 4, 045005.
- [12] M. Hörteis, J. Bartsch, S. Binder, A. Filipovic, J. Merkel, V. Radtke, S. W. Glunz, *Prog. Photovoltaics* **2010**, 18, 240.
- [13] C. Ou, L. Zhang, Q. Jing, V. Narayan, S. Kar-Narayan, *Adv. Electron. Mater.* **2020**, 6, 1900720.
- [14] D. Jahn, R. Eckstein, L. M. Schneider, N. Born, G. Hernandez-Sosa, J. C. Balzer, I. Al-Naib, U. Lemmer, M. Koch, *Adv. Mater. Technol.* **2018**, 3, 1700236.
- [15] E. S. Rosker, M. T. Barako, E. Nguyen, D. DiMarzio, K. Kisslinger, D. W. Duan, R. Sandhu, M. S. Goorsky, J. Tice, *ACS Appl. Mater. Interfaces* **2020**, 12, 29684.
- [16] M. S. Saleh, J. Li, J. Park, R. Panat, *Addit. Manuf.* **2018**, 23, 70.
- [17] Y. Gu, D. Gutierrez, S. Das, D. R. Hines, *J. Micromech. Microeng.* **2017**, 27, 097001.
- [18] M. Smith, Y. S. Choi, C. Boughey, S. Kar-Narayan, *Flexible Printed Electron.* **2017**, 2, 015004.
- [19] R. R. Tafoya, E. B. Secor, *Flexible Printed Electron.* **2020**, 5, 015009.
- [20] R. Salary, J. P. Lombardi, P. K. Rao, M. D. Poliks, *J. Manuf. Sci. Eng.* **2017**, 139, 101010.
- [21] R. R. Tafoya, E. B. Secor, *Flexible Printed Electron.* **2020**, 5, 035004.
- [22] E. B. Secor, *Flexible Printed Electron.* **2018**, 3, 035007.
- [23] J. Q. Feng, *Aerosol Sci. Technol.* **2019**, 53, 45.
- [24] L. Li, E. B. Secor, K.-S. Chen, J. Zhu, X. Liu, T. Z. Gao, J.-W. T. Seo, Y. Zhao, M. C. Hersam, *Adv. Energy Mater.* **2016**, 6, 1600909.
- [25] E. B. Secor, M. H. Dos Santos, S. G. Wallace, N. P. Bradshaw, M. C. Hersam, *J. Phys. Chem. C* **2018**, 122, 13745.
- [26] E. B. Secor, B. Y. Ahn, T. Z. Gao, J. A. Lewis, M. C. Hersam, *Adv. Mater.* **2015**, 27, 6683.
- [27] E. B. Secor, P. L. Prabhumirashi, K. Puntambekar, M. L. Geier, M. C. Hersam, *J. Phys. Chem. Lett.* **2013**, 4, 1347.